



CHORUS

This is the accepted manuscript made available via CHORUS. The article has been published as:

Pressure-induced superconductivity in the hydrogen-rich
pseudobinary $\text{CaB}_{1-x}\text{H}_x$ compounds

Wen-Hua Yang, Wen-Cai Lu, Wei Qin, Hui-Juan Sun, Xu-Yan Xue, K. M. Ho, and C. Z. Wang
Phys. Rev. B **104**, 174106 — Published 15 November 2021

DOI: [10.1103/PhysRevB.104.174106](https://doi.org/10.1103/PhysRevB.104.174106)

Pressure induced superconductivity in hydrogen-rich pseudo-binary CaB-H_n compounds

Wen-Hua Yang,^a Wen-Cai Lu,^{*ab} Wei Qin,^a Hui-Juan Sun,^a Xu-Yan Xue,^a

^aCollege of Physics, Qingdao University, Qingdao, Shandong 266071, P. R. China

^bInstitute of Theoretical Chemistry, Jilin University, Changchun, Jilin 130021, P. R. China

K. M. Ho^c and C. Z. Wang^{*c}

^cAmes Laboratory-U.S. DOE and Department of Physics and Astronomy, Iowa State University, Ames, IA 50011, U.S.A

Abstract

The crystal structures of CaB-H_n compounds with n=1-12 in a pressure range of 50-300 GPa were studied using genetic algorithm (GA) method and first-principles density function theory (DFT) calculations. Stable structures with stoichiometry of CaBH₆ and CaBH₇ were predicted in different pressure range. BH₄, BH₅ and BH₆ units were found to be the main motifs in these compounds. Moreover, metastable *Imm2* CaBH₇ is dynamically stable above 180 GPa, with the formation of tetrahedral BH₄ unit surrounded by Ca atom and H₃ unit. Electron-phonon coupling calculations reveal that the superconducting properties are closely related to the strong hydrogen-boron bonding of the BH₄ unit in *Imm2*, and T_c can reach ~200 K at 200 GPa. As the major units, BH₄, BH₅ and BH₆ units exist in the *Imm2*, *P₂* and *P2₁/m* phases of CaBH₇ at 300 GPa, respectively, the corresponding EPC parameter λ decreases with the increase of hydrogen content in CaBH₇.

*Corresponding author. Email: wangcz@ameslab.gov; wencailu@jlu.edu.cn

I. Introduction

Due to its high Debye temperature and strong electron-phonon coupling, high pressure metallic phase of hydrogen is considered a potential high temperature superconductor. However, hydrogen is expected to metallize around 450 GPa which is difficult to achieve at the current laboratory conditions [1]. Hydrogen-rich compounds can become metallic and superconducting at lower pressures in comparison with pure hydrogen phases [2], because of “chemical compression”. A recent breakthrough in discovery of superconducting hydrogen-rich compounds is the observation of high temperature superconductivity ($T_c \sim 287$ K) in carbonaceous sulfur hydride compounds under high pressure (267 GPa) [3]. A high T_c of about 200 K at a pressure of 200 GPa has also been predicted for hydrogen sulfides and confirmed by experiments [4-6]. Drozdov *et al.* [7] have also synthesized lanthanum hydride by laser heating to lanthanum in hydrogen atmosphere under 170 GPa, and showed that LaH_{10} has superconducting behavior at 250 K at 170 GPa. Evidence for superconductivity above 260 K in lanthanum superhydride at 180-200 GPa was also reported by Somayazulu *et al.* [8]. Moreover, CaH_6 , MgH_6 , YH_{10} , and LaH_{10} , have been predicted to have possible high- T_c superconductivity in the range 235 K-326 K at the pressure of 150 -300 GPa [9-12].

While binary hydrides have been investigated intensively by experimental synthesis and computational predictions, structures and superconductivity of ternary hydrides have also attracted considerable attentions [13-20]. We note that ternary compounds containing both hydrogen and boron elements have also been studied [21-23]. HBS [21] is shown to be stable above 25 GPa. It exhibits diverse phases from semiconductor to metal as the pressure increase, and becomes superconductor with a T_c of 0.8 and 1.9 K at 300 and 400 GPa, respectively. Due to strong hydrogen-boron bonding, metallic Li_2BH_6 [22] displays a critical superconducting temperature T_c of ~ 100 K between 100 and 200 GPa. Recently, theoretical investigations have also been devoted to exploring the superconducting properties in ternary La-B-H compounds [24-26]. These studies made significant progress in searching for superconductors at high pressure. In particular, ref. 25 showed that an H-rich LaBH_8 with a $Fm\bar{3}m$

symmetry exhibits an estimated superconducting T_c of 156 K at 55 GPa. It also showed that B-H bond is stronger than that of H-H in this structure, and the B atoms accommodate all the H atoms to form BH_8 units.

In addition to the hydride compounds discussed above, compounds contain Ca and B have also been investigated for possible superconductivity. At ambient pressure, simple hexagonal CaB_2 structure, which exhibit high density-of-states at the Fermi level, is predicted to be a superconductor with a T_c of 50 K [27]. *Imma* CaB with a zigzag boron chain was predicted to be a superconductor with a T_c of ~6 K at 20 GPa [27]. It is also interesting to note that both Ca atom and B atom can form stable hydrides, respectively. Ca-H and B-H compounds have also attracted a lot of attentions in the research for superconducting materials [10, 28-32]. For example, crystal structure of B_2H_6 with a *Pbcn* symmetry becomes a superconductor with a T_c of 125 K at high pressure (360 GPa) [28]. CaH_6 with the H-clathrate structure was predicted to have a T_c of 235 K at 150 GPa [10]. Recently, calcium borohydrides have investigated under the high pressure. $Pa\bar{3}$ $CaBH_6$ and *Pm* $Ca_2B_2H_{13}$ were predicted to have the T_c of 119 K and 89 K respectively at 300 GPa [33].

Considering that higher hydrogen content in many hydride compounds was predicted to give higher T_c values and Ca-B compounds also exhibit superconductivity. In this paper, we performed an extensive structural search for H-rich $CaB-H_n$ ternary compounds with $n=1-12$ in a pressure range of 50-300 GPa. The results showed that $CaB-H_n$ with odd H stoichiometry (e.g. $CaBH_7$, $CaBH_9$ and $CaBH_{11}$) is more stable. $CaBH_6$ and $CaBH_8$ is the stable compounds with the even H stoichiometry. BH_3 , BH_4 , BH_5 , BH_6 and BH_8 units were found to be the major motifs in of these $CaB-H$ compounds, and these BH_n unites play a critical role in enhancing the electron-phonon coupling and the superconductivity in these compounds. The superconducting T_c values estimated using the McMillan formula are 96 K and 190 K, respectively, for $R\bar{3}m$ $CaBH_6$ and *Imm2* $CaBH_7$ compounds at 200 GPa, and 146-162 K for the *Fm* $\bar{3}m$ $CaBH_8$ phase at 300 GPa.

II. Computational methods

Genetic algorithm (GA) search combined with first-principles density functional theory (DFT) calculations were employed to determine the low-enthalpy structures of CaB-H_n compounds under high pressure. The unbiased global structural search based on GA method combined with first-principles structural relaxation is very effective to search a large structural phase space, which has been extensively applied to the structural prediction of crystals and clusters [31]. Candidate structures obtained from the GA search were further refined using the DFT calculations. The GA search is proceeded as follows: (i) structural search started from the 60 initial random structures; (ii) using the simple cut-and-paste method, 15 offspring structures were generated at each GA generation based on the 60 parent structures; (iii) by checking enthalpies of the 75 structures, 60 low-enthalpy structures will evolve into next generation of GA. In this work, we performed 40 generations for each GA search. In the DFT structure optimizations and total energy calculations, the Cambridge Serial Total Energy Package (CASTEP) [34] was used. The ultrasoft pseudopotentials (USP) [35] and generalized gradient approximation (GGA) with Perdew-Burke-Ernzerhof (PBE) [36] functional to treat exchange and correlation energy were adopted. The electron wave functions were expanded by a basis set of plane waves with an energy cutoff of 1000 eV. Monkhorst-Pack Brillouin sampling with k-point resolution of $2\pi \times 0.02 \text{ \AA}^{-1}$ was used. The convergence criterion is 0.02 meV/atom for the total energy and 0.05 eV/Å for the forces on the atoms. The phonon spectrum and electron-phonon coupling (EPC) calculations were performed using the Quantum-ESPRESSO package [37]. Ultrasoft pseudopotentials and the plan-wave cutoff energy of 80 Ry on the kinetic energy and 800 Ry on the charge density were adopted in the calculations. The EPC parameters were calculated using $4 \times 4 \times 4$ and $5 \times 5 \times 4$ q-point meshes for $R\bar{3}m$ CaBH_6 , and $Imm2$ CaBH_7 , respectively. Denser k-point meshes, $16 \times 16 \times 16$ and $20 \times 20 \times 16$ for $R\bar{3}m$ CaBH_6 and $Imm2$ CaBH_7 were used for convergence checks for the EPC parameter λ .

III. Results and discussions

A. Structures

We performed the structural search for the CaB-H_n (n=1-12) at selected pressures of 50, 100, 150, 200, 250 and 300 GPa, respectively, as summarized in Fig. 1. We also adopt the $Fm\bar{3}m$ structure predicted for LaBH₈ by ref 25 and replace La with Ca to generate a $Fm\bar{3}m$ CaBH₈. DFT calculations show that the P_1 and Pm CaBH₈ are more stable in the pressure of 50-200 GPa, while the $Fm\bar{3}m$ CaBH₈ becomes more stable above 209 GPa (Fig. S1 [38]). The energetic stabilities of various CaB-H_n (n=1-12) compounds are evaluated through their formation enthalpies with respect to the products of dissociation into CaB and solid hydrogen at 50-300 GPa, as depicted in Fig. 2. The formation enthalpy ΔH_f is given by $\Delta H_f = [H(\text{CaBH}_n) - H(\text{CaB}) - nH(\text{H})] / (n + 2)$. The stable structures of H₂ were taken from the work of ref [39], and those of CaB were taken from the work of refs [27] and [40]. Structures with ΔH_f on the convex hull are thermodynamically stable with respect to dissociation into other structures with nearby stoichiometries, while those with ΔH_f above the convex hull are unstable or metastable. We found that the most H-rich CaB-H_n compounds with odd H stoichiometries are more stable than those with even H stoichiometries in the whole pressure range studied. In addition to CaBH₃ [33] and CaBH₅ [33], other compounds (i. e. CaBH [33], CaBH₂, CaBH₆, CaBH₇, CaBH₈, CaBH₉ and CaBH₁₁) are also predicted to be stable under selected pressures. The most stable CaBH₃ and CaBH₅ phases lie on the convex hulls at the pressure range of 50-300 GPa. CaBH becomes stable at 100 GPa, and remains stable at 100-300 GPa. $P\bar{3}m1$ CaBH₂, Pm CaBH₉ and Cm CaBH₁₁ are stable at 50 GPa and in the range of 50-200 GPa, respectively. With increasing pressure, we can see that the formation enthalpies of CaBH₆ CaBH₇ and CaBH₈ compounds approach the convex hull from the above and land on the convex hull at 200 GPa and higher pressure. The structure parameters of the low-enthalpy CaB-H_n compounds obtained from our study are listed in Table S1.

Fig. 3 shows the structures of the stable and metastable CaB-H_n compounds at various pressures. $P\bar{3}m1$ CaBH₂ at 50 GPa (Fig. 3 (a)) consists of the puckered BH layers. The H atom and Ca atoms in the structure are accommodated between two puckered layers. As the ratio of H_n increases, quasi-planar BH₃, tetrahedral BH₄, triangular bipyramids BH₅, octahedron BH₆ and cube BH₈ motifs emerged in the CaB-H_n compounds. CaBH₆ is the most stable compound among those with even H stoichiometry. In addition, CaBH₆ with a $C2/m$ symmetry is most stable at 50 GPa, in which the tetrahedral BH₄ and octahedron BH₆ units are intercalated with Ca atom and H₂ molecule (the H-H bond length is 0.797 Å), as shown in Fig. 3 (b). As the pressure increases, the $R\bar{3}m$ phase shown in Fig. 3 (c) becomes more stable for CaBH₆ when the pressure is above 292 GPa (Fig. S4). In the $R\bar{3}m$ structure at 300 GPa, each B atom has six H neighbors forming a B-H octahedron. As the H content further increases, tetrahedral BH₄ appears to be the major motif for $C2/m$, P_1 and P_2 CaBH₇ in the low pressure, as shown in Fig. 3, The BH₄ unit is separated by Ca and H atoms as well as H₂ molecule (the H-H bond length in the H₂ is 0.756Å, 0.787Å and 0.761Å at 50 GPa, respectively). The electron localization function from H₂ unit is about 1.0 (Fig. 5), indicating a strong H-H covalent bond. For P_1 and P_2 CaBH₇ phases, which transition pressures occur on 66 GPa and 90 GPa (Fig. S6), respectively. With the pressure increasing to 263 GPa, two competitive phases appear in CaBH₇, one is the $P2_1/m$ phase with the BH₆ unit (Fig. 3(h)), the distance between the remaining H atom and BH₆ is only 0.982 Å at 300 GPa; the other is the $Imm2$ phase with BH₄ and H₃ unit (Fig. 3(g)), the bond length of H-H of H₃ unit is 0.951 Å at 300 GPa. At the same time, a BH₅ unit appears in P_2 phase at 300 GPa (Fig. 3(i)), which is formed by the combination of BH₄ unit and H atom. For CaBH₈, P_1 and Pm with BH₄ units are more stable in the pressure of 50-200 GPa, as shown in Fig. S1. With the pressure increasing to 209 GPa, $Fm\bar{3}m$ CaBH₈ with BH₈ motif as shown in Fig. 3 (j) is most stable, in which the B-H bond length in the BH₈ unit is 1.248 Å. For CaBH₉, the most stable structure is the Pm structure shown in Fig. 3 (k). In this CaBH₉ structure,

tetrahedral BH_4 is still the main motif, surrounded by H_2 units and Ca atom as well as H atom. In a highly H-rich situation, CaBH_{11} (Fig. 3 (l)-(n)) becomes stable in a triclinic structure (Cm) at 50 GPa and transforms to a P_{1a} phase around 63 GPa (Fig. S7), and then to a P_{1b} phase above 272 GPa. H_2 units and H_3 chain coexist in the Cm and P_{1a} structures of CaBH_{11} under lower pressure, but only H_2 units prevail in the P_{1b} CaBH_{11} under high pressure of 300 GPa. Moreover, the tetrahedral BH_4 unite in the lower pressure Cm and P_{1a} structures transfer to quasi-planar BH_3 motif at 300 GPa.

We also examine the thermodynamic stability of the ternary Ca-B-H compounds at 50 and 300 GPa including the competitions from the known stable binary phases, as shown in Fig. S8. Structures located on the convex hull as shown in Fig. S8 are thermodynamically stable with respect to dissociation into other structures at nearby stoichiometries. We show that $P\bar{a}3\text{CaBH}_6$ from the ref [33] is about 77 meV/atom above the convex hull at 300 GPa. Although $R\bar{3}m\text{CaBH}_6$ and $P2_1/m$ (or $Imm2$) CaBH_7 from our present search are metastable phases, the formation energies of these structures are only 10 meV/atom and 12 meV/atom (or 13 meV/atom) above the convex hull at 300 GPa. These metastable compounds would be synthesized by experiment. We also proposed several possible synthesis reactions to produce CaBH_6 and CaBH_7 compounds. These synthesis reactions together with their heat of formation are listed in Table S2. Under these reaction paths, CaBH_6 and CaBH_7 always possess favorable (positive) heat of formation at 300 GPa. These energetic results for the proposed reactions provide helpful guidance to further experimental synthesis studies.

Due to the light mass of hydrogen, considering zero-point energy (ZPE) is essential for the structural stability of hydrogen-rich compound [39]. ZPE correction for the CaBH_6 , CaBH_7 and CaBH_{11} systems (Fig. S4, S6 and S7), as well as for CaB and H, were calculated within the quasiharmonic approximation at 50-300 GPa. As shown in Fig.S4, with considering ZPE contributions, the transition pressure reduced

from 292 GPa to 283 GPa for $C2/m$ to $R\bar{3}m$ CaBH_6 . For CaBH_7 (Fig. S6), P_1 , P_2 and $P2_1/m$ become stable at 67, 91 and 250 GPa, respectively. For CaBH_{11} (Fig. S7), P_{1a} and P_{1b} become stable at 53 and 272 GPa, respectively. Overall the stability of the predicted phases does not change much. Therefore, we do not consider ZPE corrections to the results presented in this paper.

B. Electronic properties

The electronic band structures and electronic densities-of-states (DOS) of the CaBH_n compounds are calculated and shown in Fig. 4 and Figs. S9-S11 respectively. Both $C2/m$ and $R\bar{3}m$ CaBH_6 are good metals at 50- 300 GPa. Several bands touching the Fermi level are seen in Fig 4 for these structures at 200 GPa. These unique band dispersion contribute larger DOS around the Fermi level which is beneficial to enhancing the superconductivity of the compounds. For CaBH_7 , $C2/m$ at 50 GPa and P_2 phase at 100-250 GPa are semiconducting with band gaps of 1.192 eV and 0.614-0.350 eV (Fig. S9), respectively. Therefore, these compounds do not exhibit superconductivity below 250 GPa. At 300 GPa, the band of P_2 CaBH_7 compound crosses the Fermi level along the G-F and Z-G directions, leading to a metallic feature (Fig.S9). By contrast, $Imm2$ and $P2_1/m$ CaBH_7 exhibit strong metallic features as can be seen from Fig. 4 (c) and (d), respectively. Higher electronic DOS near the Fermi energy level contributes to the relative high superconducting T_c of these two compounds (see Table 1). From the local DOS analysis, we see that the H-1s state provides the largest contribution to the DOS near the Fermi level (especially for the $R\bar{3}m$ CaBH_6) as shown in Fig. 4.

We also found that Pm CaBH_9 and P_{1b} CaBH_{11} display semiconducting character with indirect-band-gaps which change from 1.633 to 0.144 eV in Pm CaBH_9 and from 2.474 to 0.122 eV in P_{1b} CaBH_{11} when the pressures increases from 50 to 200 GPa (Fig. S10-S11), respectively. For CaBH_9 , the band dispersion crosses the Fermi level at the A point as shown in Fig. 4(e), leading to a weak metallic state when the pressure is above 200 GPa. However, the DOS at the Fermi level is too small to lead to any significant superconductivity. For CaBH_{11} at 300 GPa, one narrow band crosses the

Fermi level near the F and Q points and lays about 1 eV above the Fermi level between these two K points so it contributes very little to the DOS at the Fermi level. Surprisingly, the superconducting T_c of this compound above 250 GPa is significant (about 120 K, see Table 1) although the DOS at the Fermi level is not high. This would be due to the strong electron-phonon coupling strength in this system.

We also calculated the electron localization functions (ELF) for ternary CaBH_6 and CaBH_7 compounds. As shown in Fig. 5, the ELF values of B-H in BH_6 or BH_4 units in CaB-H ($n=6$ and 7) are $0.65\sim 0.75$, indicating their covalent characters. The ELF values of H-H in H_2 and H_3 units for these structures are very high (close to 1), indicating that they are strong covalent bond. While the ELF values for the Ca atoms are close to 0, implying that Ca-H is ionic bond. The Bader charge calculation shows the Ca atoms in the CaBH_6 ($R\bar{3}m$ and $C2/m$) and CaBH_7 ($Imm2$ and $P2_1/m$) act as electron donors, which donate $1.39e/1.42e$ and $1.41e/1.46e$ at 300 GPa, BH_4 , BH_6 and H_2 (or H_3) units are acceptors.

C. Superconducting properties

We also explore possible superconductivity in the CaB-H compounds at different pressure by calculating the logarithmic average phonon frequency ω_{\log} , the electron-phonon coupling (EPC) parameter λ , and the electronic DOS at the Fermi level, $N(E_f)$ (Table I). For Pm CaBH_9 at 250 GPa, ω_{\log} is 1046 K and the λ is only 0.16. The small value of λ makes the T_c in CaBH_9 close to 0 K. By contrast, the calculated λ and ω_{\log} values are 0.94 (1.02) and 1467 K (1057 K) for $R\bar{3}m$ CaBH_6 (or $C2/m$) at 200 GPa, the correspondingly T_c values are 76-91 K (67-76 K) according to the McMillan equation. We also performed phonon and EPC calculations for the Pm and the $Fm\bar{3}m$ CaBH_8 . The calculated EPC parameters, λ , for the Pm at 200 GPa and $Fm\bar{3}m$ at 300 GPa are 0.99 and 1.31, respectively, which give T_c values of 63-74 K and 146-162 K, respectively. As the EPC parameter λ is larger than 1.5, which represents very strong electron phonon coupling for systems. The McMillan equation

[45] needs to be corrected by including two correction factors f_1 and f_2 ,

$$T_c = \frac{f_1 f_2 \omega_{\log}}{1.20} \exp\left[\frac{-1.04(1+\lambda)}{\lambda(1-0.62\mu^*)-\mu^*}\right],$$

which represent the strong coupling and the shape correction, respectively. In our work, for the *Imm2* and *P2₁/m* CaBH₇ at 200 GPa and *P1_b* CaBH₁₁ at 300 GPa, the EPC parameters λ are much higher than the other CaB-H ternary compounds, which are 2.80, 1.69, and 1.75 respectively. The final corrected T_c values are about 184-190 K, 136-151 K, for *Imm2* and *P2₁/m* CaBH₇ at 200 GPa, and 112-128 K for *P1_b* CaBH₁₁ at 300 GPa, respectively.

Fig. 6 show the phonon dispersions and the projected phonon density of states, Eliashberg spectral function $\alpha^2 F(\omega)$, and the electron phonon coupling integral, $\lambda(\omega)$ for CaB-H compounds. We found that the electron-phonon coupling of CaB-H compounds is mainly from hydrogen-boron bonding within the BH_n units. For *C2/m* and *R $\bar{3}m$* CaBH₆, there is no imaginary frequency in the phonon dispersion curves under the given pressures, suggesting the dynamical stability of these compounds. For *R $\bar{3}m$* CaBH₆, vibrations of Ca atom (below 15 THz) contribute 14% of the total λ , whereas the remaining 86% comes from vibration modes of BH₆ unit. Similarly, the B-H vibration modes of BH₄ and BH₆ units from *C2/m* CaBH₆ also donate about 60% of the total λ . For *P1_b* CaBH₁₁, the optical modes are mainly from the Ca atom. The low-frequency (below 14 THz) modes are associated with Ca atom, which contribute about 31% of the total λ . The intermediate frequencies (between 14 and 18 THz) come mainly from the vibrations of quasi-planar BH₃ unit, including a small amount vibration modes of Ca atom and H₂ units, which contribute only 13 % of the total λ . The frequency intervals greater than 18 THz are origin from the B-H modes of BH₃ unit and H-H modes of molecular H₂ units, which contribute 56 % of total λ .

Due to the strong electron-phonon coupling, the *Imm2* CaBH₇ has a high T_c , which value is about 184-190 K at 200 GPa. At 200 GPa (Fig. 6), the low-frequency vibration modes (below 13 THz) are mainly from the vibrations of Ca atom and H₃

unit, with some amount vibration intensity from the tetrahedral BH_4 unit, which contribute about 33% of total λ . The high frequency modes (> 24 THz) are originated from the BH_4 and H_3 units, which contribute 29% of λ . The intermediate frequency bands (between 13 and 24 THz) are originated from the vibrations of the tetrahedral BH_4 , which contribute about 38 % of the total value of λ . As pressure increases to 250 (or 300 GPa), the calculated ω_{\log} for the *Imm2* CaBH_7 increase to 1026 K (or 1062 K), $N(E_f)$ increase to 6.85 (or 7.05). The responsible λ is 2.14 (or 2.22), which indicate the strong electron-phonon coupling. And we found that the contribute of the B-H vibration modes from BH_4 unit to the total λ increases to 48% at 250 GPa and 52% at 300 GPa, respectively. Similarly, we also found that BH_5 and BH_6 units play an important role for EPC of P_2 and $P2_1/m$ CaBH_7 , as shown in Fig. 6(e) and (f). BH_4 , BH_5 and BH_6 units are the major units in the *Imm2*, P_2 and $P2_1/m$ phases of CaBH_7 at 300 GPa. We found that when the number of H atoms in the BH_n unit increases from 4 to 6 in the *Imm2* to the $P2_1/m$ phases, the corresponding EPC parameter λ decreases from 2.22 to 1.29. This observation suggest that although BH_n unites in CaBH_7 compounds are essential for achieving superconductivity, too many H atoms in a BH_n unit may reduce the strength of the EPC parameter λ in CaBH_7 , thus reduce the superconducting T_c .

IV. Conclusions

In summary, we have explored the crystal structures and electron properties of the H-rich CaB-H_n compounds under high pressure by GA search in combination with first principles DFT calculations. The results showed that the H-rich CaBH_n compound with odd H stoichiometry (e.g. CaBH_7 , CaBH_9 and CaBH_{11}) is more stable. CaBH_6 and CaBH_8 are the stable compounds with the even H stoichiometry. BH_3 , BH_4 , BH_5 , BH_6 and BH_8 units were found to be the major motifs in of these CaB-H compounds. Among these compounds, metastable phase *Imm2* from CaBH_7 was found to be dynamically stable above 180 GPa, and it exhibits strong electron-phonon coupling which drives the superconducting T_c up to ~ 200 K at 200 GPa. The high T_c in this compound is closely related to the strong electron-phonon coupling, which is

mainly from hydrogen-boron bonding within the BH_4 unit. Our results will provide a guidance for the experimental work on discovery of novel superconductor in CaB-H compounds.

Acknowledgments

This work was supported by the National Natural Science Foundation of China (Grant No. 21773132, No. 12004210 and No. 21603114); Natural Science Foundation of Shandong Province (Grant No. ZR2020MB046); the Higher Educational Science and Technology Program of Shandong Province of China (Grant No. J17KA179). Work at Ames Laboratory was supported by the U.S. Department of Energy (DOE), Office of Science, Basic Energy Sciences, Materials Science and Engineering Division including a grant of computer time at the National Energy Research Scientific Computing Centre (NERSC) in Berkeley, CA. Ames Laboratory is operated for the U.S. DOE by Iowa State University under contract # DE-AC02-07CH11358.

References

- [1] C. Narayana, H. Luo, J. Orloff, and A. L. Ruoff, *Nature* **393**, 46 (1998).
- [2] N. W. Ashcroft, *Phys Rev Lett* **92** 187002 (2004).
- [3] E. Snider, N. Dasenbrock-Gammon, R. McBride, M. Debessai, H. Vindana, K. Vencatasamy, K. V. Lawler, A. Salamat, and R. P. Dias, *Nature* **586**, 373 (2020).
- [4] A. P. Drozdov, M. I. Eremets, I. A. Troyan, V. Ksenofontov, and S. I. Shylin, *Nature* **525**, 73 (2015).
- [5] D. F. Duan, Y. X. Liu, F. B. Tian, D. Li, X. L. Huang, Z. L. Zhao, H. Y. Yu, B. B. Liu, W. J. Tian, and T. Cui. *Sci. Rep.***4**, 6968 (2014).
- [6] D. F. Duan, X. L. Huang, F. B. Tian, D. Li, H. Y. Yu, Y. X. Liu, Y. B. Ma, B. B. Liu, and T. Cui. *Phys Rev B*, **91**, 180502 (2015).
- [7] A. P. Drozdov, P. P. Kong, V. S. Minkov, S. P. Besedin, M. A. Kuzovnikov, S. Mozaffari, L. Balicas, F. F. Balakirev, D. E. Graf, and V. B. Prakapenka, E. Greenberg, D. A. Knyazev, M. Tkacz, *Nature*, **569**, 528 (2019).
- [8] M. Somayazulu, M. Ahart, A. K. Mishra, Z. M. Geballe, M. Baldini, Y. Meng, V. V. Struzhkin, and R. J. Hemley, *Phys. Rev. Lett.*, **122**, 027001 (2019).

- [9] X. L. Feng, J. R. Zhang, G. Y. Gao, H. Y. Liu, and H. Wang, *Rsc Adv* **5**, 59292 (2015).
- [10] H. Wang, J. S. Tse, K. Tanaka, T. Iitaka, and Y. M. Ma, *P Natl Acad Sci USA* **109**, 6463 (2012).
- [11]. H. Y. Liu, I. I. Naumov, R. Hoffmann, N. W. Ashcroft and R. J. Hemley. *Proc. Natl. Acad. Sci. USA*. **114**, 6990 (2017).
- [12] F. Peng, Y. Sun, C.J. Pickard, R. J. Needs, Q. Wu, Y. M. Ma. *Phys. Rev. Lett.* **119**, 107001 (2017).
- [13] D. Z. Meng, M. Sakata, K. Shimizu, Y. Iijima, H. Saitoh, T. Sato, *Phys. Rev. B*, **99**, 024508 (2019).
- [14] M. Rahm, R. Hoffmann, and N. W. Ashcroft. *J. Am. Chem. Soc.*, **139**, 8740 (2017).
- [15] S. T. Zhang, L.T. Zhu, H. Y. Liu, and G. C. Yang, *Inorg. Chem.*, **55** 11434 (2016).
- [16] Y. B. Ma, D. F. Duan, Z. J. Shao, H. Y. Yu, H. Liu, F. B. Tian, X. L. Huang, D. Li, B. B. Liu, and T. Cui. *Phys. Rev. B*, **96** 144518 (2017).
- [17] Y. B. Ma, D. F. Duan, Z. J. Shao, D. Li, L. Y. Wang, H. Y. Yu, F. B. Tian, H. Xie, B. B. Liu, and T. Cui, *Phys. Chem. Chem. Phys.* **19**, 27406(2017).
- [18] X. W. Liang, A. Bergara, L. Y. Wang, B. Wen, Z. S. Zhao, X. F. Zhou, J. L. He, G. Y. Gao, and Y. J. Tian, *Phys. Rev. B*, **99**, 100505 (2019).
- [19] Da. Li, Y. Liu, F. B. Tian, S. L. Wei, Z. Liu, D. F. Duan, B. B. Liu, T. Cui, *Front. Phys.* **13**, 137107 (2018).
- [20] X. W. Liang, S. T. Zhao, C. C. Shao, A. Bergara, H. Y. Liu, L. Y. Wang, R. X. Sun, *Phys. Rev. B*, **100**, 184502 (2019).
- [21] X. Du, S. T. Zhang, J. Y. Lin, X. H. Zhang, A. Bergaram and G. C. Yang. *Phys. Rev. B*, **100**, 134110 (2019).
- [22] C. Kokail, W. Linden, and L. Boeri, *Phys. Rev. Mater*, **1**, 074803 (2017).
- [23] Y. Sun, J. Lv, Y. Xe, H. Y. Lu, and Y. M. Ma, *Phys. Rev. Lett.*, **123**, 097001 (2019).
- [24] S. D. Catado, C. Heil, W. Linden and L. Boeri, *Phys. Rev. B*, **104**, L020511 (2021).

- [25] X. W. Liang, A. Bergara, X. D. Wei, L. Y. Wang, R. X. Sun, H. Y. Liu, R. J. Hemley, L. Wang, G. Y. Gao, Y. J. Tian, Phys. Rev. B, **104**, 134501 (2021).
- [26] S. D. Cataldo, W. Linden, and L. Boeri, arXiv: 2106.07266 (2021).
- [27] S. Shah and A. N. Kolmogorov, Phys. Rev. B, **88**, 014107 (2013).
- [28] H. J. Choi, S. G. Louie, and M. L. Cohen, Phys. Rev. B, **80**, 064503 (2009).
- [29] Y. Yao and R. Hoffmann, J. Am. Chem. Soc., **133**, 21002 (2011).
- [30] C. H. Hu, A. R. Oganov, Q. Zhu, G. R. Qian, G. Frapper, A. O. Lyakhov, and H. Y. Zhou, Phys. Rev. Lett., **110**, 165504 (2013).
- [31] W. H. Yang, W. C. Lu, S. D. Li, X. Y. Xue, Q. J. Zang, K. M. Ho, and C. Z. Wang, Phys. Chem. Chem. Phys., **21**, 5466 (2019).
- [32] Z. J. Shao, D. F. Duan, Y. B. Ma, H. Y. Yu, H. Song, H. Xie, D. Li, F. B. Tian, B. B. Liu, and T. Cui, Inorg. Chem. **58**, 2558 (2019).
- [33] S. D. Catakdi, W. Linden, and L. Boeri, Phys. Rev. B, **102**, 014516(2020).
- [34] V. Milman, B. Winkler, J.A. White, C.J. Pickard, M.C. Payne, E.V. Akhmatkaya, R.H. Nobes, Int. J. Quantum Chem. **77**, 895(2000).
- [35] Vanderbilt, D. Phys. Rev. B, **41**, 7892 (1990).
- [36] Perdew, J. P.; Burke, K.; Ernzerhof, M. Phys. Rev. Lett., **77**, 3865 (1996).
- [37] P. Giannozzi, S. Baroni, N. Bonini, M. Calandra, R. Car, C. Cavazzoni, G. L. Chiarotti, M. Cococcioni, I. Dabo, A. Dal Corso, *et al.* J. Phys.: Condens. Matter, **21**, 395502 (2009).
- [38] See Supplemental Material for Crystal structure information; calculated formation enthalpy, electronic band structures and phonon dispersions, 2D-ELF and ternary phase diagram for all predicted CaB-H compounds, which includes Refs. [10, 25, 27-31, 39-44].
- [39] C. J. Pickard and R. J. Needs. Nat Phys, **3**, 473 (2007).
- [40] At the pressure of 50 GPa, CaB is found to be stable with *Imma* symmetry [27]. Under high pressure, we performed the structural search for the CaB at selected pressures of 100, 150, 200, 250 and 300 GPa, respectively, we found that *Imma* CaB still retains stable till 195 GPa, *C2/m* CaB becomes stable above 195 GPa. The corresponding structural information are given in Table S1.

- [41] J. S. Tse, D. D. Klug, S. Desgreniers, J. S. Smith, R. Flacau, Z. Liu, J. Hu, N. Chen, D. T. Jiang, *Phys. Rev. B.*, **75**, 134108 (2007).
- [42] Y. W. Li, B. Li, T. Cui, Y. Li, L. J. Zhang, Y. M. Ma, G. T. Zou, *J. Phys.: Condens. Matter*, **20**, 045211 (2008).
- [43] A. R. Oganov, J. H. Chen, C. Gatti, Y. Z. Ma, Y. M. Ma, C. W. Glass, Z. X. Liu, T. Yu, O. O. Kurakevych, and V. L. Solozhenko, *Nature*, **457**, 863 (2009).
- [44] Yao, Y, Klug, D. D, Sun, J. Marto, M. *Phys. Rev. Lett.* **103**, 055503 (2009).
- [45] P. B. Allen and R. Dynes. *Phys. Rev. B*, **12**, 905 (1975).
- .

Table 1 Calculated electron-phonon coupling parameters (λ), the logarithmic Average phonon frequency ω_{\log} (K), electronic density of states at the Fermi level $N(E_f)$ (in states/Ry) and superconducting critical temperatures T_c (K) for the CaB-H compounds at selected pressures.

Structure	Space group	Pressure (GPa)	λ	$N(E_f)$	ω_{\log}	T_c (K)
						$\mu = 0.13 \sim 0.1$
CaBH ₂	$P\bar{3}m1$	100	0.20	2.28	1158	0
	P_3	50	1.01	4.77	752	46-53
	$R\bar{3}m$	200	0.94	9.14	1467	76-91
		250	0.92	9.08	1585	80-95
CaBH ₆	$C2/m$	300	0.91	9.07	1631	83-98
		100	0.98	10.25	825	48-56
		200	1.02	9.76	1057	67-76
	$Imm2$	300	1.12	9.44	1168	84-96
		200	2.80	6.76	822	184-190
		250	2.14	6.85	1026	168-184
CaBH ₇	$P2_1/m$	300	2.22	7.05	1062	183-200
		150	1.34	6.08	1286	117-135
		200	1.69	6.11	1025	136-151
	P_2	300	1.29	6.33	1380	121-135
		300	1.64	6.54	954	123-136
CaBH ₈	Pm	150	0.86	2.80	1037	46-55
		200	0.99	2.73	1076	63-74
	$Fm\bar{3}m$	250	1.44	3.88	1524	152-167
		300	1.31	3.74	1635	146-162
CaBH ₉	Pm	250	0.20	0.55	1046	0
		300	0.36	0.91	905	1-2
CaBH ₁₁	$P1b$	250	1.75	3.73	822	112-123
		300	1.60	3.91	937	112-128

Figure captions

FIG. 1 Stable phases of CaB-H compounds with respect to CaB (*Imma* and *C2/m*) and H₂ (*P6₃/m*, *C2/c* and *Cmca* 12) at the different pressures. *Fm $\bar{3}m$* CaBH₈, CaB and H₂ are from the refs 25, 27, 39 and 40, respectively.

Fig. 2 Calculated formation enthalpies (in eV/atom) of CaB-H compounds with respect to CaB (*Imma* and *C2/m*) and H₂ (*P6₃/m*, *C2/c* and *Cmca* 12) at the different pressures. CaBH_{1,3,5}, CaBH₈ (*Fm $\bar{3}m$*), CaB and H₂ are from the refs 33, 25, 27, 39 and 40, respectively.

FIG. 3 Predicted crystal structures of CaB-H compounds at high pressure. (a) *P $\bar{3}m$ 1*CaBH₂ at 50 GPa. (b) *C2/m* CaBH₆ at 50 GPa, (c) *R $\bar{3}m$* CaBH₆ at 200 GPa, (d) *C2/m* CaBH₇ at 50 GPa. (e) *P₁* CaBH₇ at 50 GPa, (f) *P₂* CaBH₇ at 100 GPa, (g) *Imm2* CaBH₇ at 300 GPa, (h) *P2₁/m* CaBH₇ at 300 GPa, (i) *P₂* CaBH₇ at 300 GPa, (j) *Fm $\bar{3}m$* CaBH₈ at 250 GPa. (k) *Pm* CaBH₉ at 50 GPa. (l) *Cm* CaBH₁₁ at 50 GPa. (m) *P_{1a}* CaBH₁₁ at 100 GPa and (n) *P_{1b}* CaBH₁₁ at 300 GPa. The blue, green and pink spheres represent the Ca, B and H atoms, respectively.

FIG. 4. Electronic band structures and density of states of CaB-H compounds. (a) *R $\bar{3}m$* CaBH₆ at 200 GPa, (b) *C2/m* CaBH₆ at 200 GPa, (c) *Imm2* CaBH₇ at 200 GPa, (d) *P2₁/m* CaBH₇ at 200 GPa, (e) *Pm* CaBH₉ at 250 GPa and (f) *P_{1b}* CaBH₁₁ at 300 GPa.

FIG. 5. 2D-ELF of CaB-H compounds. (a) and (d) *R $\bar{3}m$* CaBH₆ on the (110) and (0 $\bar{1}$ 3) planes, respectively. (b) *Imm2* CaBH₇ on the (100) plane. (c) *P2₁/m* CaBH₇ on the (001) plane, (e) and (f) *C2/m* CaBH₆ on the (001) and (010) planes, respectively.

FIG. 6. Calculated phonon band structures, phonon density of states, the Eliashberg phonon spectral function, $\alpha^2 F(\omega)$, and the partial electron-phonon intergral, $\lambda(\omega)$ for CaB-H compounds. (a) *R $\bar{3}m$* CaBH₆ at 200 GPa, (b) *C2/m* CaBH₆ at 200 GPa, (c) *P_{1b}* CaBH₁₁ at 300 GPa, (d) *Imm2* CaBH₇ at 200 GPa, (e) *P₂* CaBH₇ at 300 GPa and (f) *P2₁/m* CaBH₇ at 300 GPa.

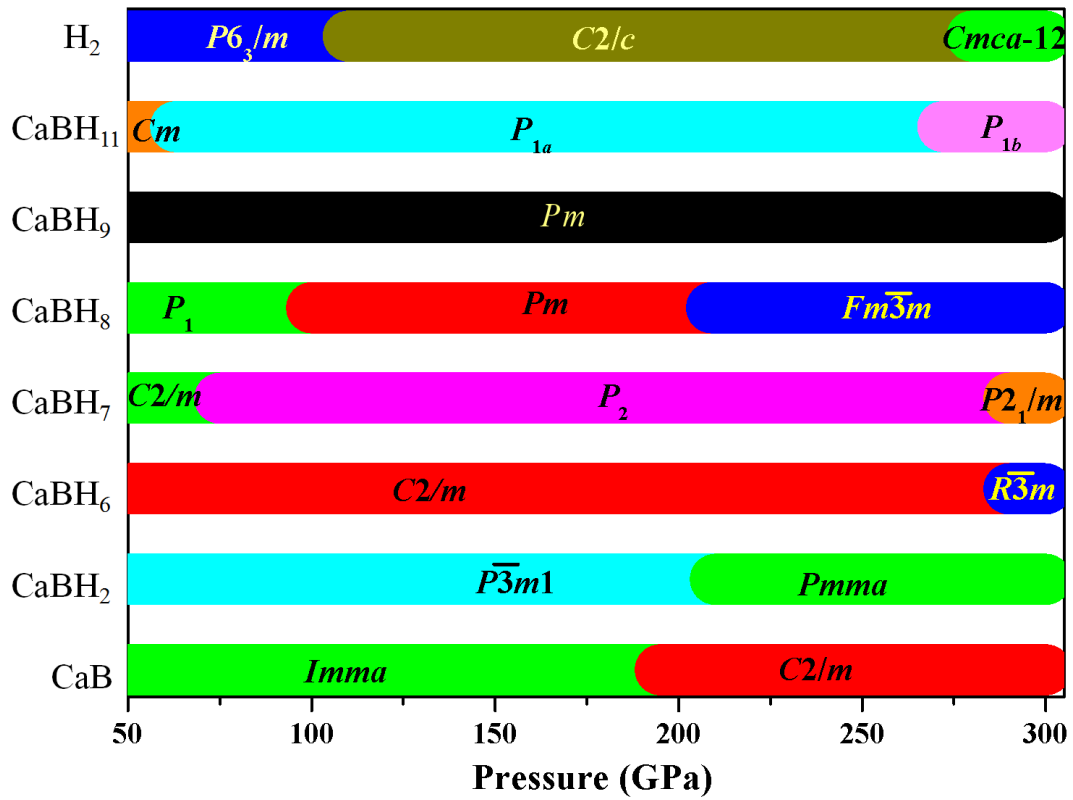


FIG. 1 Stable phases of CaB-H compounds with respect to CaB ($Imma$ and $C2/m$) and H₂ ($P6_3/m$, $C2/c$ and $Cmca-12$) at the different pressures. $Fm\bar{3}m$ CaBH₈, CaB and H₂ are from the refs 25, 27, 39 and 40, respectively.

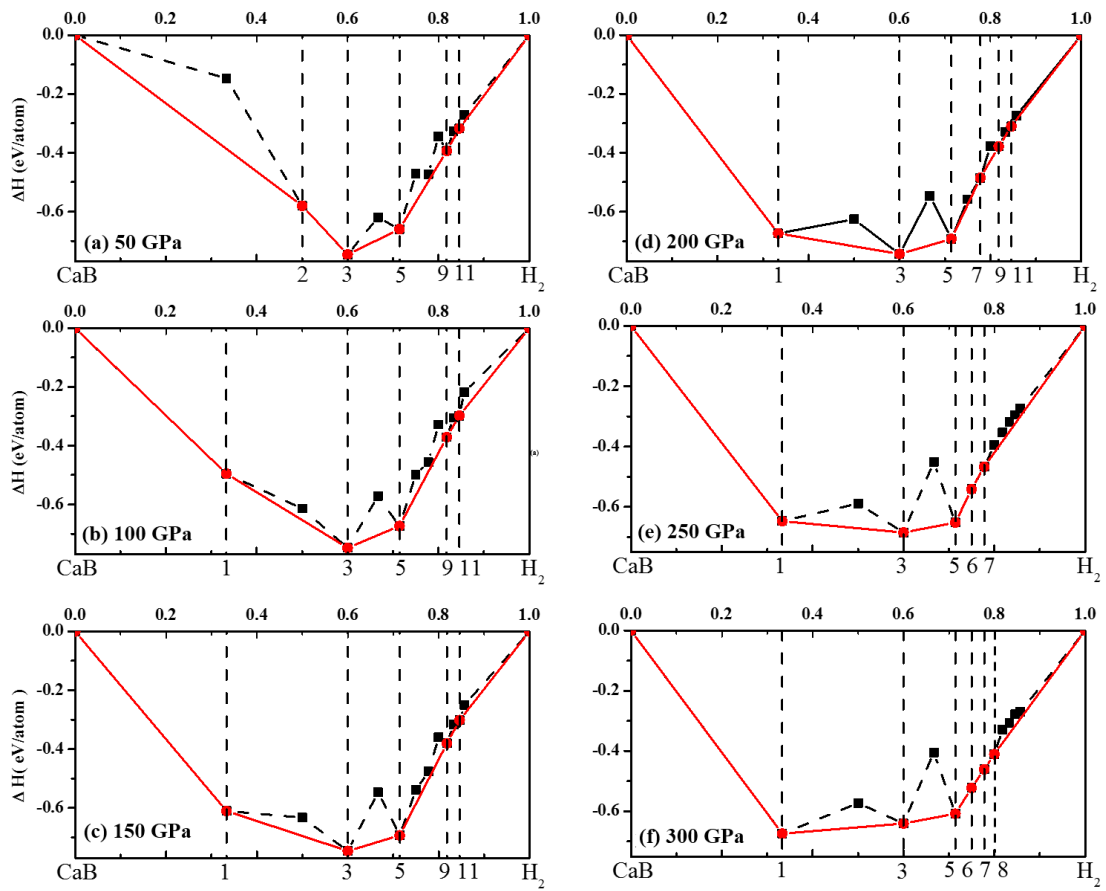


Fig. 2 Calculated formation enthalpies (in eV/atom) of CaB-H compounds with respect to CaB (*Imma* and *C2/m*) and H_2 (*P6_3/m*, *C2/c* and *Cmca* 12) at the different pressures. CaBH_{1,3,5}, CaBH₈ (*Fm $\bar{3}m$*), CaB and H_2 are from the refs 33, 25, 27, 39 and 40, respectively.

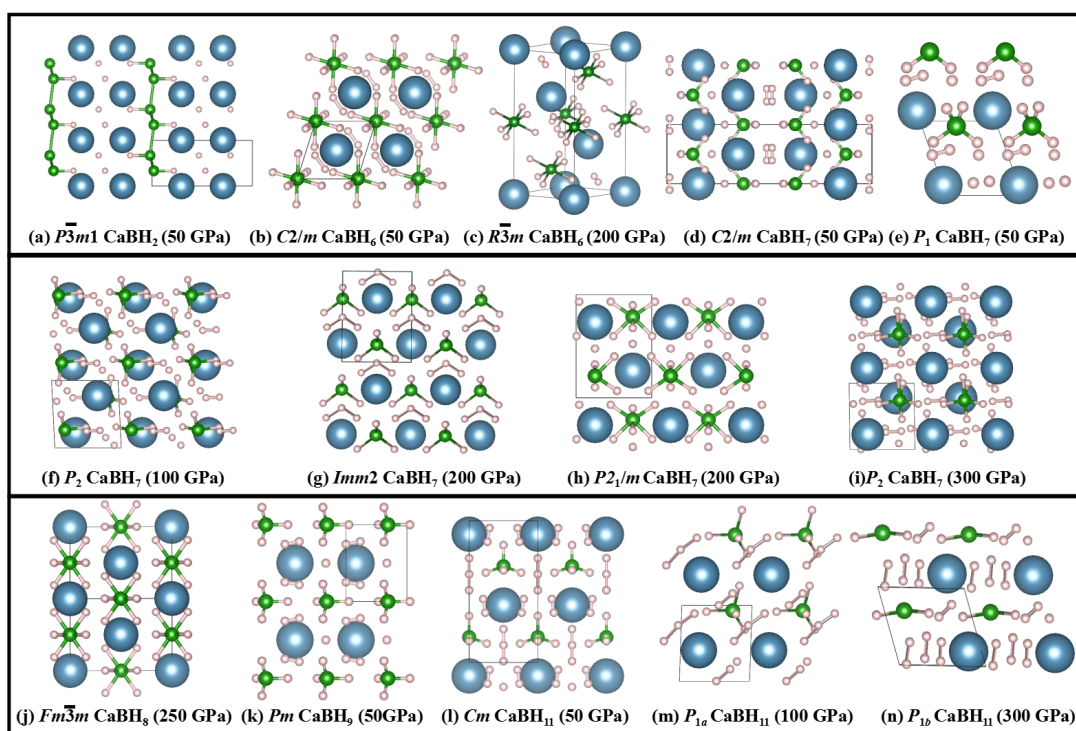


FIG. 3 Predicted crystal structures of CaB-H compounds at high pressure. (a) $P\bar{3}m1$ CaBH₂ at 50 GPa. (b) $C2/m$ CaBH₆ at 50 GPa, (c) $R\bar{3}m$ CaBH₆ at 200 GPa, (d) $C2/m$ CaBH₇ at 50 GPa. (e) P_1 CaBH₇ at 50 GPa, (f) P_2 CaBH₇ at 100 GPa, (g) $Imm2$ CaBH₇ at 200 GPa, (h) $P2_1/m$ CaBH₇ at 200 GPa, (i) P_2 CaBH₇ at 300 GPa, (j) $Fm\bar{3}m$ CaBH₈ at 250 GPa. (k) Pm CaBH₉ at 50 GPa. (l) Cm CaBH₁₁ at 50 GPa. (m) P_{1a} CaBH₁₁ at 100 GPa and (n) P_{1b} CaBH₁₁ at 300 GPa. The blue, green and pink spheres represent the Ca, B and H atoms, respectively.

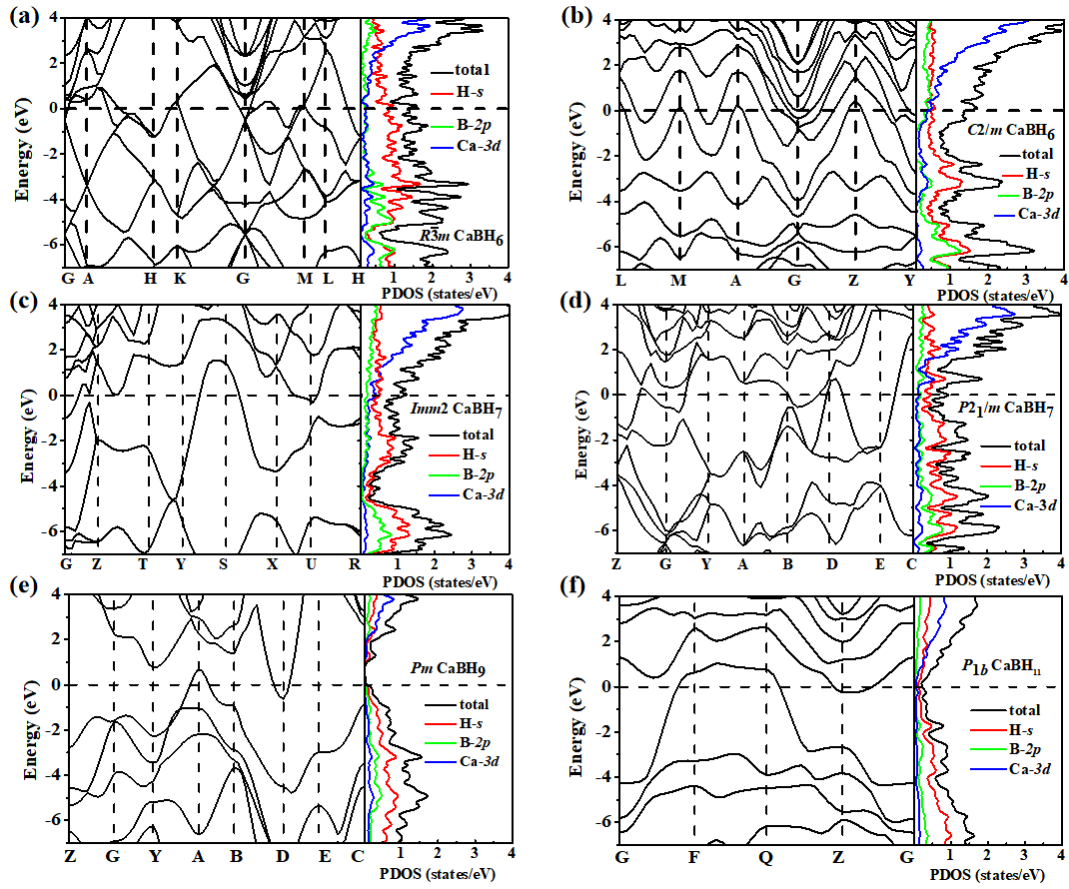


FIG. 4 Electronic band structures and density of states of CaB-H compounds. (a) $R\bar{3}m$ CaBH₆ at 200 GPa, (b) $C2/m$ CaBH₆ at 200 GPa, (c) $Imm2$ CaBH₇ at 200 GPa, (d) $P2_1/m$ CaBH₇ at 200 GPa, (e) Pm CaBH₉ at 250 GPa and (f) $P1_b$ CaBH₁₁ at 300 GPa.

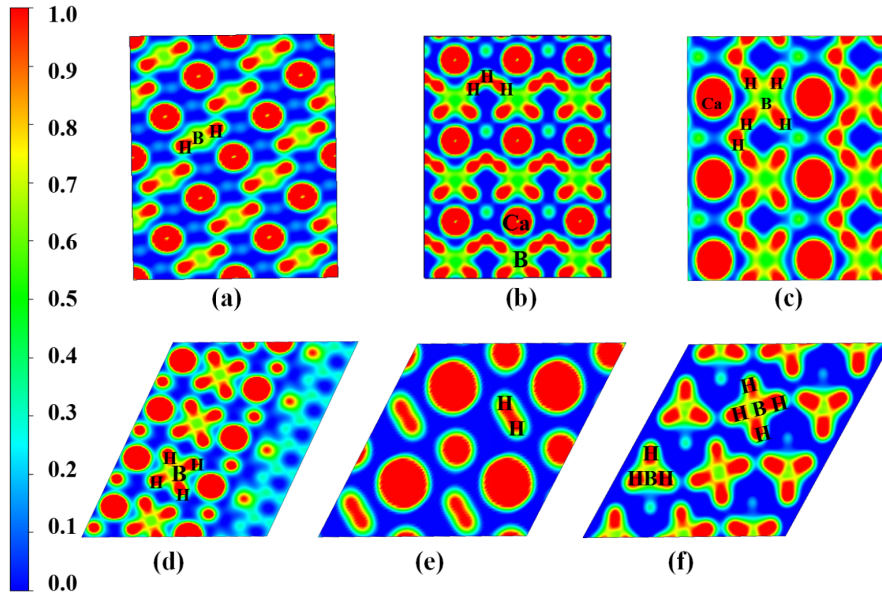


FIG. 5. 2D-ELF of CaB-H compounds. (a) and (d) $R\bar{3}m$ CaBH_6 on the (110) and $(0\bar{1}3)$ planes, respectively. (b) $Imm2$ CaBH_7 on the (100) plane. (c) $P2_1/m$ CaBH_7 on the (001) plane, (e) and (f) $C2/m$ CaBH_6 on the (001) and (010) planes, respectively.

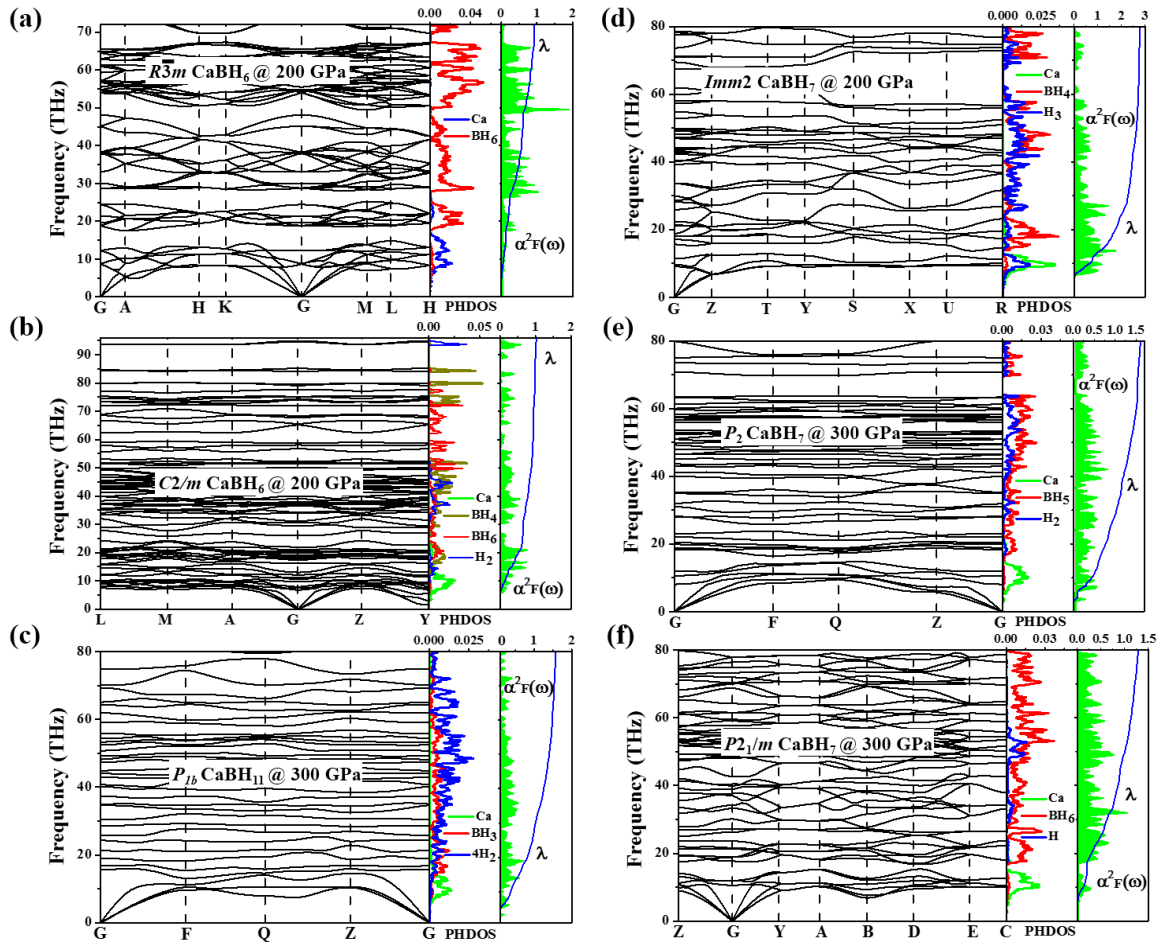


FIG. 6 Calculated phonon band structures, phonon density of states, the Eliashberg phonon spectral function $\alpha^2 F(\omega)$, and the partial electron-phonon intergral, $\lambda(\omega)$ for CaB-H compounds. (a) $R\bar{3}m$ CaBH₆ at 200 GPa, (b) $C2/m$ CaBH₆ at 200 GPa, (c) $P1b$ CaBH₁₁ at 300 GPa, (d) $Imm2$ CaBH₇ at 200 GPa, (e) P_2 CaBH₇ at 300 GPa and (f) $P2_1/m$ CaBH₇ at 300 GPa.